




Irreversible multilayer adsorption of semirigid k -mers deposited on one-dimensional latticesN. De La Cruz Félix ^{1,2}, P. M. Centres,¹ A. J. Ramirez-Pastor ^{1,*}, E. E. Vogel,^{3,4} and J. F. Valdés ³¹*Departamento de Física, Instituto de Física Aplicada, Universidad Nacional de San Luis-CONICET, Ejército de Los Andes 950, D5700HHW, San Luis, Argentina*²*Departamento de Física, Instituto de Física, Facultad de Ciencias, Universidad Autónoma de Santo Domingo, Dominican Republic*³*Departamento de Física, Universidad de La Frontera, Casilla 54-D, Temuco, Chile*⁴*Center for the Development of Nanoscience and Nanotechnology (CEDENNA), 9170124 Santiago, Chile*

(Received 15 April 2020; accepted 9 June 2020; published 2 July 2020)

Irreversible multilayer adsorption of semirigid k -mers on one-dimensional lattices of size L is studied by numerical simulations complemented by exhaustive enumeration of configurations for small lattices. The deposition process is modeled by using a random sequential adsorption algorithm, generalized to the case of multilayer adsorption. The paper concentrates on measuring the jamming coverage for different values of k -mer size and number of layers n . The bilayer problem ($n \leq 2$) is exhaustively analyzed, and the resulting tendencies are validated by the exact enumeration techniques. Then, the study is extended to an increasing number of layers, which is one of the noteworthy parts of this work. The obtained results allow the following: (i) to characterize the structure of the adsorbed phase for the multilayer problem. As n increases, the $(1 + 1)$ -dimensional adsorbed phase tends to be a “partial wall” consisting of “towers” (or columns) of width k , separated by valleys of empty sites. The length of these valleys diminishes with increasing k ; (ii) to establish that this is an in-registry adsorption process, where each incoming k -mer is likely to be adsorbed exactly onto an already adsorbed one. With respect to percolation, our calculations show that the percolation probability vanishes as L increases, being zero in the limit $L \rightarrow \infty$. Finally, the value of the jamming critical exponent ν_j is reported here for multilayer adsorption: ν_j remains close to 2 regardless of the considered values of k and n . This finding is discussed in terms of the lattice dimensionality.

DOI: [10.1103/PhysRevE.102.012106](https://doi.org/10.1103/PhysRevE.102.012106)**I. INTRODUCTION**

Lattice models have played an important role in the study of the jamming and percolation phenomena [1,2]. In the most common lattice-gas picture for systems out of equilibrium, the state of sites on the lattice is changed from empty/vacancy to filled/occupied, or vice versa, randomly, sequentially, and irreversibly. This process is known as random sequential adsorption (RSA) [5–8]. More complex models take into account that large ensembles of sites can be changed simultaneously at each event. An extensive overview of this field can be found in the excellent work by Evans [6] and references therein. Experimentally, RSA has been observed in different processes, such as oxidation of one-dimensional polymer chains [9], formation of polymer brush films [10], fouling of contact lenses [11], etc.

The jamming phenomenon appears when the deposited objects cannot cover all the lattice sites due to the absence of free space of appropriate size and shape, leaving empty sites (gaps too small to fit new particles are left in the monolayer). One of the simpler cases of RSA that produces a jamming state is the deposition of dimers (objects occupying two adjacent sites when being adsorbed on the lattice) on infinite d -dimensional lattices. The coverage corresponding to the jamming state,

which is called jamming coverage, depends strongly on the size and shape of the deposited object and the lattice structure [6–8]. In general, it is quite difficult to find exact analytical solutions for the jamming coverage.

For some special types of lattices, geometrical considerations enable us to derive their jamming thresholds exactly. Thus, the jamming state has been solved analytically, and exact limit concentrations are known for linear k -mers (elements occupying k sites on the lattice) on one-dimensional lattices [12–15]. Two- and three-dimensional lattices do not present such a topological advantage, and jamming thresholds have to be estimated numerically by means of computer simulations [16–29].

If the concentration of the deposited objects on the substrate exceeds a critical value, a cluster (a group of occupied sites such that each site has at least one occupied nearest-neighbor site) extends from one side of the system to the other, determining a phase transition in the system. This transition, known as the percolation phase transition, is a geometrical phase transition where a critical concentration (or percolation threshold) separates a phase of finite clusters from a phase where an infinite cluster is present [1–4]. Thus, the jamming coverage has an important role in the percolation threshold, and the interplay between RSA and percolation is relevant for the description of various deposition processes. The RSA of dimers on one-dimensional lattices is the simplest example of the competition between percolation and jamming. Pictorially,

*Author to whom correspondence should be addressed: antorami@unsl.edu.ar

a jamming state of dimers consists of strings with an even number of occupied sites that are separated by vacant sites. Accordingly, there will be no one island that could connect the opposite extremes of the system.

So far most of the studies of percolation and jamming have considered the adsorption up to the monolayer. However, multilayer adsorption is an experimentally as well as theoretically relevant field of surface science due to its importance for the characterization of solid surfaces [30]. Moreover, several experiments on adhesion of colloidal particles on solid substrates have reported the formation of multilayer deposits in essentially irreversible deposition processes from unstable or marginally stable colloid suspensions [31–36].

In equilibrium, various approximations and models have been proposed to describe multilayer adsorption. Brunauer-Emmett-Teller (BET) [37] and Frenkel-Halsey-Hill (FHH) [38–40] theories are the simplest, and they provided the basis for more elaborate approaches accounting for lateral interaction between the adsorbed molecules, differences between the adsorption energy and the structure between the first and upper layers, surface heterogeneity, etc. These leading models, along with more recent contributions [41–44], have played a central role in the characterization of solid surfaces by means of gas adsorption.

In the case of irreversible multilayer adsorption, the inherent complexity of the system still represents a major difficulty in the development of approximate and numerical solutions. However, several attempts were made in the past to solve the k -mer irreversible multilayer adsorption problem. Among them, Bartelt and Privman [45] formulated a model of irreversible multilayer adsorption on homogeneous one-dimensional substrates. Combining the exact results on monolayer adsorption and the approximate treatment of higher-layer effects, closed-form analytical results were derived for several quantities of interest. In Refs. [46–49], some other variants of the problem were explored: the effect of diffusional relaxation, different deposition mechanisms, continuum deposition, etc.

Despite the results mentioned above, there are still many open questions in the field of irreversible multilayer adsorption. The objective of this paper is to provide a thorough report based on different and complementary methods, testing them first in the better known bilayer case increasing both the length of the deposited k -mer and the length L of the one-dimensional lattice on which the depositions occur. This allows us later to pile up further layers, building up a “wall” of deposited objects, growing in a different direction in a different way [(1 + 1)-dimensional growth process], with restricted possibilities of relaxing particles from upper to lower layers in neighboring layers. This adds a new parameter to the analysis: the number of layers or coats. The resulting scheme allows us to address new questions in this field, such as the efficiency in the coverage, the possibility of percolation, and the size of the islands or patches at the different layers. Regarding the last point, the obtained results indicate that, as k -mer size and the number of layers increase, the adsorption process occurs via an in-registry adsorption process, where an incoming k -mer tends to be adsorbed exactly onto an already adsorbed one. Accordingly, the structure of the adsorbed phase can be thought of as an array of columns of width k separated by

valleys of empty sites. As k increases, the separation distance between columns diminishes. This phenomenon has already been studied for the case of equilibrium multilayer adsorption [42–44]. The numerical simulations will be complemented by statistical techniques such as those coming from finite-size scaling (FSS) theory. In addition, the tendencies of the bilayer will also be validated by exact results for small lattices obtained by exact enumeration of states in configurational space.

Finally, the accurate determination of the jamming critical exponent ν_j revealed a simple dependence of this quantity on the dimensionality of the lattice: $\nu_j = 2/d$, where d is the lattice dimension (in this case, $d = 1$). Thus, the maximum of the derivative of the jamming probability goes as $M^{1/2}$, where M is the number of available lattice sites. This finding, reported for multilayer adsorption, is relevant as it allows us to generalize recent results found for irreversible monolayer adsorption on Euclidean and fractal lattices [50].

The paper is organized as follows. The model and simulation scheme are described in Sec. II. Results are presented and discussed in Sec. III. The conclusions are drawn in Sec. IV. Finally, Appendix contains the exact results for small lattices coming from a complete enumeration of configurations.

II. THE MODEL AND BASIC DEFINITIONS

The most common parameter to characterize the kinetic properties of a deposition process is the coverage $\theta(t)$, defined as the ratio of the number of occupied sites at time t with respect to the total number of sites. As mentioned in Sec. I, the final state generated by irreversible adsorption is a disordered state (known as a jamming state), where only gaps too small to accept new particles are left in the monolayer. The coverage at this final state is $\theta(t \rightarrow \infty) \equiv \theta^j$. In the case of multilayer deposition, the index n is added to denote that the quantity corresponds to the n th layer, θ_n^j , counting from bottom to top.

The inherent complexity of the system still represents a major difficulty in the development of accurate analytical solutions for $\theta(t)$ (and θ_n^j), so computer simulations are a very important tool for studying this subject. Basically, the model proposed here consists of adsorption of semirigid k -mers on a one-dimensional lattice of size L in $d = 1 + 1$ dimensions in the way it was explained in the Introduction. Then, starting from an initially empty lattice, the k -mers are horizontally (or left to right) sent randomly toward the surface following a RSA process (similar to a rain of horizontal rods). The k -mers can be adsorbed according to the following rules (examples are given in Fig. 1): (i) particles do not shrink, so each particle of any k -mers has its own horizontal coordinate; (ii) particles can partially stretch (the k -mers can bend to accommodate themselves to the roughness of the surface (substrate and/or previous depositions) as far as stretching between consecutive atoms does not go over $\sqrt{2}$ interatomic distances [see Fig. 1(b)], allowing for up to a difference of one vertical position between consecutive particles (the difference between the vertical coordinates of consecutive particles within any k -mer cannot be more than |1|); (iii) a k -mer is accepted for deposition only if it is in full contact with the substrate or lower layers without leaving empty spaces underneath (bridges or cantilevers with two or more empty spaces below

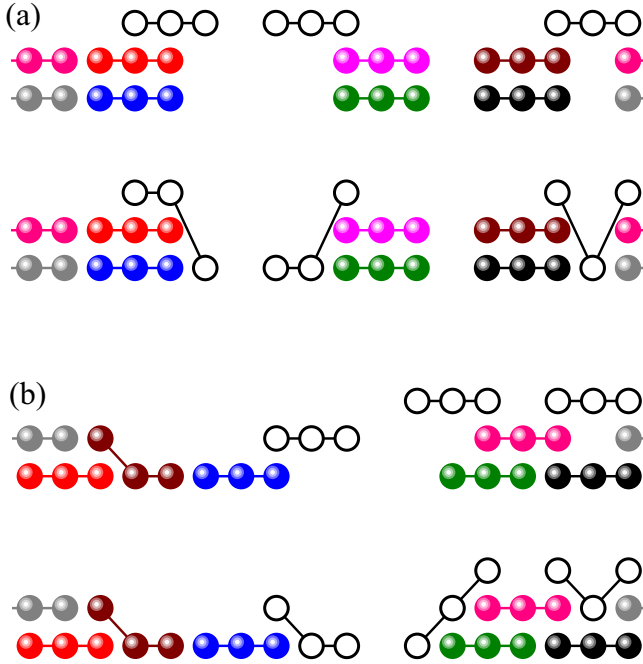


FIG. 1. Examples of trimer ($k = 3$) depositions on a lattice with $L = 18$ and periodic boundary conditions. Solid symbols joined by lines correspond to trimers previously deposited onto the lattice. Open circles joined by lines represent trimers attempting to deposit on the substrate. (a) Not allowed configurations. (b) Allowed configurations. Top and bottom panels show the incoming trimers arriving to the interface and occupying their final positions, respectively.

are forbidden); and (iv) periodic boundary conditions are used in all the layers, so that all sites are statistically equivalent (this condition is valid for simulating large systems where the ends make negligible differences).

As was previously defined, the deposition process is left to continue until saturation is reached for a prefixed number of layers n_t . Then, the coverage in the n th layer is determined as

$$\begin{aligned} \theta_n &= \frac{\text{number of occupied sites on the } n\text{th layer}}{L} \\ &= \frac{N_n}{L}, \end{aligned} \quad (1)$$

and the total coverage is

$$\begin{aligned} \theta_{\text{total}} &= \frac{\text{total number of occupied sites}}{n_t L} \\ &= \frac{\sum_{n=1}^{n_t} N_n}{n_t L} = \frac{1}{n_t} \sum_{n=1}^{n_t} \theta_n. \end{aligned} \quad (2)$$

To better understand the spectral behavior of the coverage per layer, we will obtain histograms for the different layers. For this purpose, the range $0 \leq \theta_n \leq 1$ is swept for the n th layer, by range index i , defining bins of width $2 \times \Delta\theta$. Then, we measure the value of the coverage per layer at the position i , $\theta_{n,i}$, and the corresponding absolute frequency of occurrence, $\phi_{n,L,k}^{\text{abs}}(\theta_{n,i})$. From there we can continue to define the cumulative relative frequency corresponding to the n th layer, $\Phi_{n,L,k}(\theta_n)$. The procedure is as follows:

(i) Starting from an initially empty lattice, the k -mers are deposited according to the RSA mechanism described at the beginning of this section. Adsorption of k -mers continues until the saturation of a prefixed number of layers n_t . (n_t represents the maximum number of layers in our simulations. To avoid spurious effects in the upper layers, our measurements are performed between $n = 1$ and $n = n_t - k$.)

(ii) The absolute frequency is calculated:

$$\phi_{n,L,k}^{\text{abs}}(\theta_{n,i}) = \begin{cases} +1, & \theta_{n,i} = \theta_{n,i} \pm \Delta\theta, \\ 0 & \text{otherwise.} \end{cases} \quad (3)$$

As mentioned above, the subscript i indicates the central value of the i th bin of the distribution.

(iii) The cumulative frequency is calculated as

$$\Phi_{n,L,k}(\theta_n) = \sum_i \phi_{n,L,k}^{\text{abs}}(\theta_{n,i}). \quad (4)$$

(iv) Finally, m runs of the steps (i)–(iii) are carried out for each lattice size L and each value of k , and the cumulative frequency is averaged on the m runs.

In our simulations, a set of $m = 10^5$ independent samples was numerically prepared for several values of $L/k = 128, 192, 256, 384, \text{ and } 640$. Within each series, the ratio L/k was kept constant to avoid spurious results due to the k -mer size in comparison with the lattice size. All of this requires extensive computer calculations.

To improve the accuracy, and using sigmoidal fitting functions, the different curves of $\Phi_{n,L,k}$ are expressed as a function of continuous values of θ_n . Thus, their derivatives behave like a Gaussian function around the maximum [17],

$$\frac{d\Phi_{n,L,k}(\theta_n)}{d\theta_n} = \frac{1}{\sqrt{2\pi} \Delta_{n,L,k}} \exp \left\{ -\frac{1}{2} \left[\frac{\theta_n - \theta_n^j(L)}{\Delta_{n,L,k}} \right]^2 \right\}, \quad (5)$$

where $\theta_n^j(L)$ is the concentration at which the slope of $\Phi_{n,L,k}(\theta_n)$ is maximum, and $\Delta_{n,L,k}$ is the standard deviation from $\theta_n^j(L)$.

According to the finite-size scaling theory, the cumulative frequency follows a scaling law given by

$$\Phi_{n,L,k}(\theta_n) = \overline{\Phi_{n,k}}(u), \quad (6)$$

where $\overline{\Phi_{n,k}}(u)$ is a scaling function and $u \equiv (\theta_n - \theta_n^j)L^{1/\nu_j}$. Based on Eq. (6), it is possible to calculate the jamming critical exponent with reasonable accuracy. Thus, the maximum of the derivative of Eq. (6) leads to

$$\left(\frac{d\Phi_{n,L,k}}{d\theta_n} \right)_{\text{max}} \propto L^{1/\nu_j}. \quad (7)$$

Another alternative way to obtain ν_j is given by the divergence of the root-mean-square deviation of the threshold observed from their average values, $\Delta_{n,L,k}$ in Eq. (5),

$$\Delta_{n,L,k} \propto L^{-1/\nu_j}. \quad (8)$$

In the next section, the cumulative frequency and its properties will be used to study the bilayer and multilayer problems.

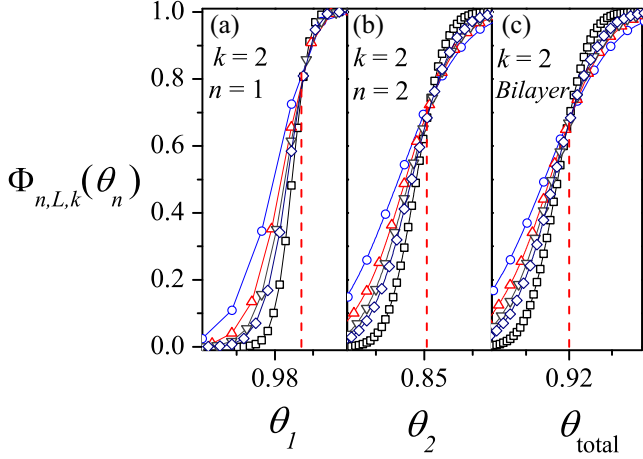


FIG. 2. Cumulative frequency $\Phi_{n,L,k}(\theta_n)$ for dimers deposition with $n \leq 2$. L/k : $L/k = 128$, circles; $L/k = 192$, up-triangles; $L/k = 256$, down-triangles; $L/k = 384$, diamonds; and $L/k = 640$, squares. (a) Data corresponding to layer 1. (b) Data corresponding to layer 2. (c) Data corresponding to layers 1 and 2 (bilayer).

III. RESULTS AND DISCUSSION

A. Bilayer adsorption model

We begin by discussing the bilayer adsorption problem ($n \leq 2$) for the case of dimers ($k = 2$). The corresponding cumulative frequency curves are shown in Fig. 2 for different values of L/k : $L/k = 128$, circles; $L/k = 192$, up-triangles; $L/k = 256$, down-triangles; $L/k = 384$, diamonds; and $L/k = 640$, squares. Parts (a), (b), and (c) present data corresponding to layer 1, layer 2, and both layers, respectively. As can be observed, all curves vary smoothly between 0 and 1, and they approach a step function when L goes to infinity. Moreover, the curves cross each other in a very well-defined interval in the θ -axis, which allows us to obtain a preliminary estimation of the jamming threshold [51]. In this case, the values obtained are $\theta_{n=1}^j = 0.987(3)$, $\theta_{n=2}^j = 0.853(3)$, and $\theta_{\text{total}}^j = 0.920(3)$. As is expected, $\theta_{\text{total}}^j = (\theta_{n=1}^j + \theta_{n=2}^j)/2$ [Eq. (2)].

A more accurate determination of $\theta_{n=1}^j$, $\theta_{n=2}^j$, and θ_{total}^j can be obtained by using an extrapolation scheme for the positions $\theta_n^j(L)$. The procedure is depicted in Fig. 3, where the values of $\theta_n^j(L)$ are shown as a function of L^{-1} for the cases presented in Fig. 2: squares, layer 1 (bottom panel); circles, layer 2 (top panel); and triangles, bilayer (middle panel). By fitting the simulation data with a linear function, the limit jamming thresholds are obtained from the values of the y-intercepts. In this case, $\theta_{n=1}^j(\infty) = 0.9853(6)$, $\theta_{n=2}^j(\infty) = 0.8505(5)$, and $\theta_{\text{total}}^j(\infty) = 0.9179(5)$.

As can be seen, there are coincidences (within numerical errors) between the results obtained from the extrapolation of $\theta_n^j(L)$ (Fig. 3) and those obtained from the intersection point of the cumulative frequency curves (Fig. 2). For the rest of the paper, we will use just one jamming threshold for each size n and k corresponding to the value obtained by extrapolation: $\theta_n^j(k)$ (for simplicity, we will drop the ∞).

By following the procedure described in the previous section, the jamming critical exponent ν_j can be calculated. Thus,

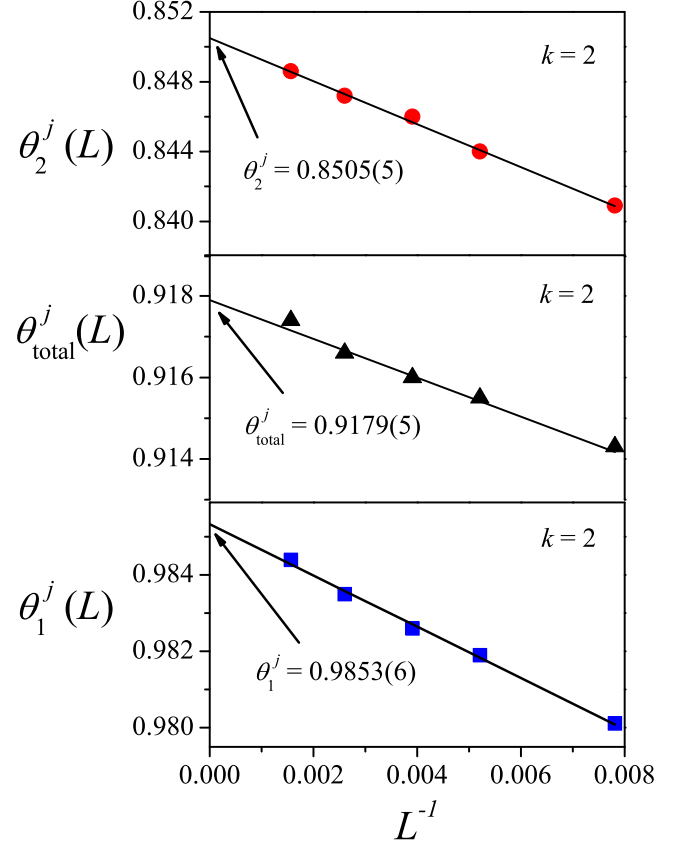


FIG. 3. Extrapolation of $\theta_{n=1}^j(L)$ (squares, bottom panel), $\theta_{n=2}^j(L)$ (circles, top panel), and $\theta_{\text{total}}^j(L)$ (triangles, middle panel) toward the thermodynamic limit. The data were obtained from the curves presented in Fig. 2.

Fig. 4(a) shows $(\frac{d\Phi_{n,L,k}}{d\theta_n})_{\text{max}}$ and $\Delta_{n,L,k}$ as a function of L/k (in a log-log graph) for the cases presented in Fig. 2. Then, exponent ν_j can be obtained from the slope of the different curves [see Eqs. (7) and (8)]. In this case, $\nu_j = 1.993(21)$ (main figure, $n = 1$), $\nu_j = 1.980(27)$ (main figure, $n = 2$), $\nu_j = 1.969(42)$ (main figure, bilayer), $\nu_j = 1.986(37)$ (inset, $n = 1$), $\nu_j = 1.973(38)$ (inset, $n = 2$), and $\nu_j = 1.969(47)$ (inset, bilayer). The study was repeated for other sizes k . In all cases, the obtained values of ν_j remain close to 2.

In a recent paper from our group [50], it was demonstrated that, for monolayer deposition, $\Delta_{n,L,k}$, $(\frac{d\Phi_{L,k}}{d\theta})_{\text{max}} \propto M^{1/2}$, where M is the number of elements (sites or nodes) that form the lattice. In the case of Euclidean and fractal lattices, where lattice side L and space dimension d can be defined, the asymptotic behavior can be written as $M^{1/2} = L^{d/2} = L^{1/\nu_j}$, with $\nu_j = 2/d$. By extending these arguments to the case of the bilayer adsorption problem, it is possible to write $M^{1/2} = L^{d/2}$ for each single layer, and $M^{1/2} = (2L)^{d/2}$ for the complete bilayer system. Then, in all cases (first layer, second layer, and entire system), it is expected that $\Delta_{n,L,k}$, $(\frac{d\Phi_{n,L,k}}{d\theta_n})_{\text{max}} \propto L^{d/2} = L^{1/\nu_j}$, with $\nu_j = 2/d$. In the particular case of the one-dimensional bilayer problem, $d = 1$ and consequently $\nu_j = 2$. The values of the jamming critical exponent obtained in Fig. 4(a) ($\nu_j \approx 2$) confirm the predictions of

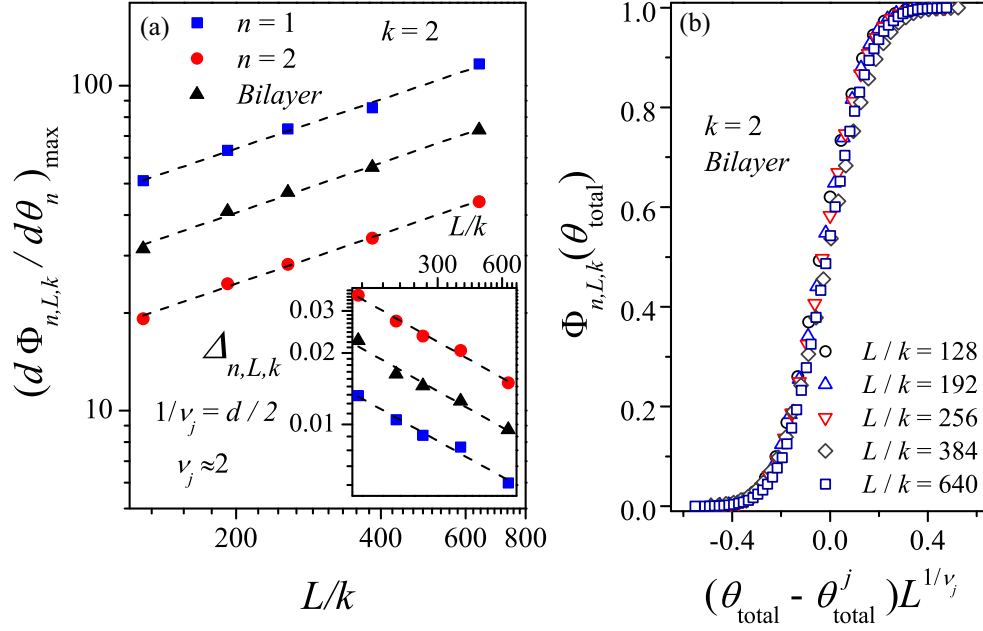


FIG. 4. (a) Log-log plots of $(\frac{d\Phi_{L,k}}{d\theta})_{\max}$ and $\Delta_{n,L,k}$ as a function of L/k for the case shown in Fig. 2. According to Eq. (7), the slope of each line corresponds to $1/v_j$ [or to $-1/v_j$ in the case of Eq. (8)]. (b) Data collapse of the cumulative frequency, $\Phi_{n,L,k}(\theta_n)$ vs $(\theta_{\text{total}} - \theta_{\text{total}}^j)L^{1/v_j}$ [Eq. (6)]. The curves were obtained using $\theta_{\text{total}}^j = 0.9179$ (see Fig. 3) and $v_j = 2$.

Ref. [50], and they validate its applicability to the multilayer deposition problem.

Scaling behavior can be further tested by plotting $\Phi_{n,L,k}(\theta_n)$ versus $(\theta_n - \theta_n^j)L^{1/v_j}$ [Eq. (6)] and looking for data collapsing. Using the values of θ_n^j calculated above and the value of the critical exponent $v_j = 2$, we obtain an excellent scaling collapse as shown in Fig. 4(b). This leads to independent controls and consistency checks of the value of jamming critical exponent.

The procedure of Fig. 3 was repeated for k ranging between 2 and 100, and the results are presented in Fig. 5. $\theta_{n=1}^j, \theta_{n=2}^j$,

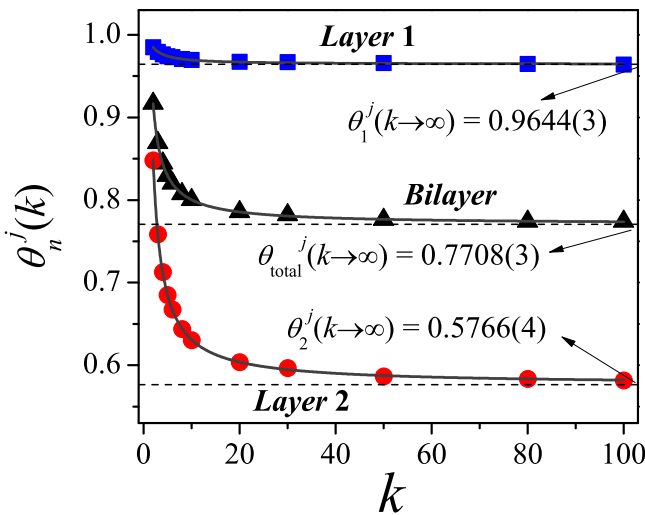


FIG. 5. Jamming coverage for layer 1, $\theta_{n=1}^j$ (squares); layer 2, $\theta_{n=2}^j$ (circles); and bilayer θ_{total}^j (triangles) as functions of k . Symbols represent simulation data, and solid lines correspond to fitting curves obtained from Eqs. (9)–(11).

and θ_{total}^j show decreasing behavior as the size k increases. A qualitatively similar tendency was observed for the monolayer problem [12–15], where θ_1^j decreases monotonically with k , and, for $k \rightarrow \infty$, the jamming threshold tends to Rényi's parking constant $\theta_1^j(k \rightarrow \infty) \rightarrow c_R \approx 0.7475979202$ [15].

In the bilayer problem, the deposited particles preferentially fill the first layer leaving empty sites, which are occupied by monomers belonging to k -mers that have relaxed from the second layer. The result is simple: on the one hand, the limit coverage of the first layer is higher than that corresponding to the monolayer problem in the entire range of k , and on the other hand, the limit coverage of the second layer is lower than that corresponding to the monolayer problem in the entire range of k .

As is standard in the literature [21,28], the simulation data can be fitted to the function $\theta_j(k) = A + B/k + C/k^2$ ($k \geq 2$). In the case of Fig. 5,

$$\theta_1^j(k) = 0.9644(3) + \frac{0.055(3)}{k} - \frac{0.027(6)}{k^2}, \quad (9)$$

$$\theta_2^j(k) = 0.5766(4) + \frac{0.545(5)}{k} - \frac{0.002(10)}{k^2}, \quad (10)$$

and

$$\theta_{\text{total}}^j(k) = 0.7708(3) + \frac{0.298(3)}{k} - \frac{0.011(7)}{k^2}. \quad (11)$$

The results from Eqs. (9)–(11) are included in Fig. 5 (solid lines). The values of A represent the limit concentrations by infinitely long k -mers. Thus, for the bilayer problem and $k \rightarrow \infty$, $\theta_1^j(k \rightarrow \infty) \approx 0.9644(3)$, $\theta_2^j(k \rightarrow \infty) \approx 0.5766(4)$, and $\theta_{\text{total}}^j(k \rightarrow \infty) \approx 0.7708(3)$. As is expected, $\theta_{\text{total}}^j = (\theta_{n=1}^j + \theta_{n=2}^j)/2$.

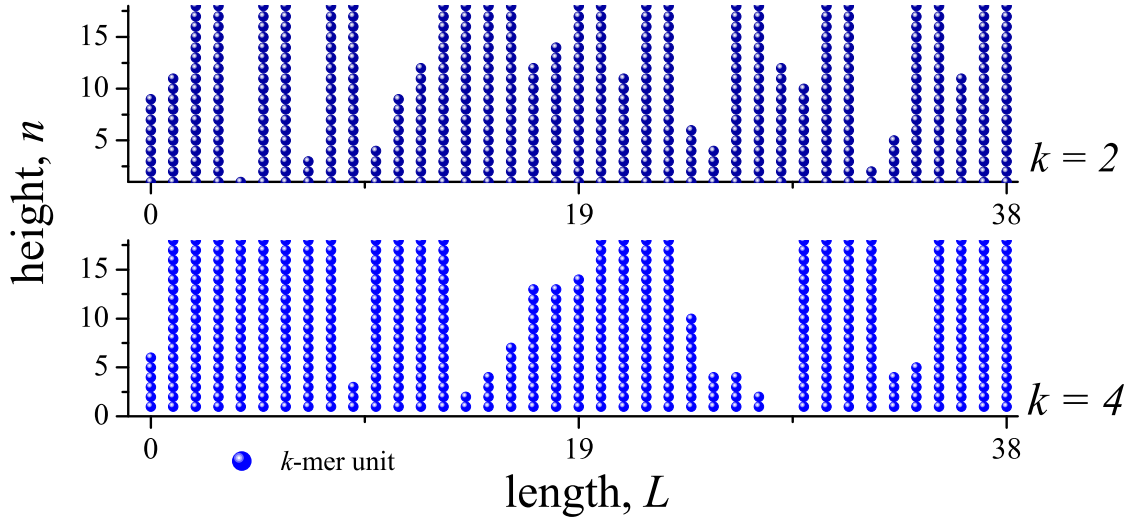


FIG. 6. Portion of a linear lattice of length $L = 38$ and height $n = 18$ for two values of k : dimers ($k = 2$, top panel) and tetramers ($k = 4$, bottom panel). As can be seen, the k -mer units tend to form islands of length k as n increases.

The value of the limit concentration obtained in Eq. (9) has important implications from the standpoint of percolation theory. In fact, this value remains below unity [$\theta_1^j(k \rightarrow \infty) \approx 0.9644 < 1$], indicating that percolation never occurs due to jamming. See more details in Appendix.

B. Multilayer adsorption model

In this section, we will analyze the RSA problem for $n > 2$. The simulations were performed for k -mers on one-dimensional L -lattices with $k = 2-224$, $L/k = 128-640$, and $n_i = 32-360$. A simple visualization of how the k -mers fill the lattice is presented in Fig. 6: case $k = 2$ (top panel) and case $k = 4$ (bottom panel). As will be discussed below, the formation of columns of width k dominates the adsorption process for long enough times.

We start by analyzing the jamming coverage for different values of k as a function of the number of layers n . The results of this study are shown in Fig. 7, which leads to the following observations: (i) all curves begin with a coverage less than 1, i.e., full coverage is not achieved for any layer; (ii) the layer coverage has a strong dependence with n , decreasing monotonically toward the upper layers; (iii) for each particle size k , the corresponding coverage curve for each n converges to an asymptotic limit: $\theta_\infty^j(k)$. In what follows, we will discuss the behavior of $\theta_\infty^j(k)$ and its implications on the properties of the adsorbed phase.

The dependence of $\theta_\infty^j(k)$ on the size k is shown in Fig. 8 (solid circles). The figure also includes the curve for $\theta_1^j(k)$ as a function of k for the one-dimensional monolayer adsorption problem (solid diamonds) [12–15]. The limit coverage increases with increasing k , and it tends to an asymptotic value for very large k -mer sizes ($k \rightarrow \infty$) $\theta_\infty^j(\infty) \approx 0.71147$, which is close to the value of Rényi’s parking constant, $c_R [= \theta_1^j(\infty)]$. This finding is a first indication that, for large k -mers, the adsorption state of the n th layer (large n) approaches from below the corresponding asymptotic limit for the monolayer problem. Accordingly, the adsorption process could be

thought of as an in-registry adsorption process, where a k -mer can adsorb exactly onto an already adsorbed one. Let us suppose a deposited k -mer denoted as A , whose units occupy sites characterized by the following pairs of (horizontal,vertical) coordinates: $(i, n_i), (i + 1, n_{i+1}), \dots, (i + k, n_{i+k})$. A k -mer B is said to be adsorbed in-registry with the previously deposited k -mer A when the coordinates of k -mer B are $(i, n_i + 1), (i + 1, n_{i+1} + 1), \dots, (i + k, n_{i+k} + 1)$. Thus, the horizontal coordinates of A and B are identical, while the vertical coordinates differ in 1. This phenomenon has already been studied for the case of equilibrium multilayer adsorption [42–44].

We have considered that the entire adsorbed phase can be studied as a set of overlapping linear lattices, each one corresponding to one of the n layers. In this way, the Hoshen and Kopelman algorithm [52] has been used to obtain the number of islands of length λ in each layer. The apparition frequency of an island of size λ in the n th layer is denoted

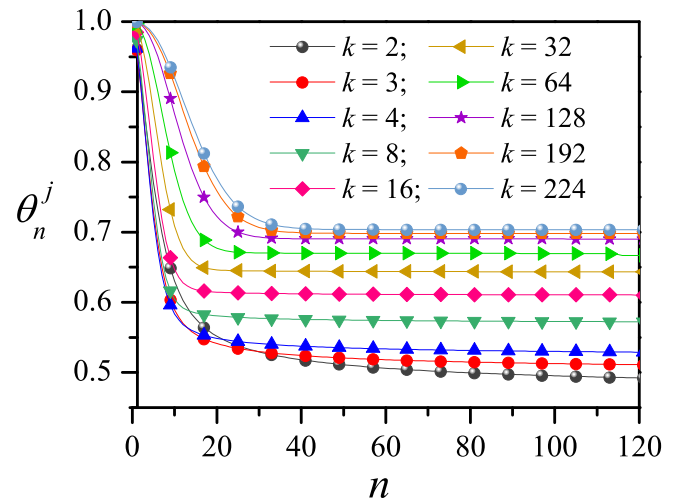


FIG. 7. Jamming coverage per layer as a function of the number of layers for different values of k as indicated.

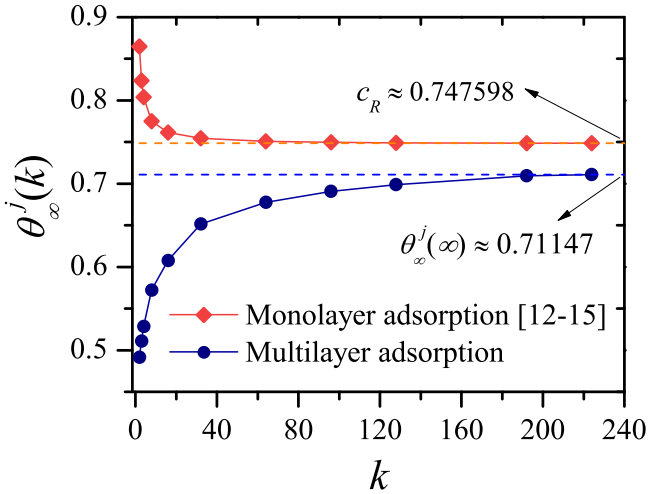


FIG. 8. $\theta_\infty^j(k)$ as a function of k (solid circles). The figure includes also the curve of jamming coverage for the one-dimensional monolayer adsorption problem (solid diamonds) [12–15].

as $f_n(\lambda)$,

$$f_n(\lambda) = \frac{\text{total number of islands of size } \lambda \text{ in the } n\text{th layer}}{\text{total number of islands in the } n\text{th layer}}. \quad (12)$$

In Fig. 9(a), the frequency $f_n(\lambda)$ is shown as a function of the size λ for three different values of k ($k = 2$, circles; $k = 4$, diamonds; and $k = 8$, triangles) and $n = 20$. The simulations were performed for $L/k = 128$ and $n_t = 64$. In part (b), the k -

mer size is set to 2 and 8, and the frequency $f_n(\lambda)$ is calculated for different values of n as indicated. The following results can be obtained from the figure:

- (i) $f_{n=20}(\lambda)$ is different from 0 for $\lambda = sk$ ($s = 1, 2, 3, \dots$).
- (ii) $f_{n=20}(\lambda = 2) \approx 0.8178$, $f_{n=20}(\lambda = 4) \approx 0.1318$, $f_{n=20}(\lambda = 6) \approx 0.0312$, and $f_{n=20}(\lambda > 6) \approx 0$ for $k = 2$; $f_{n=20}(\lambda = 4) \approx 0.9453$, $f_{n=20}(\lambda = 8) \approx 0.0384$, and $f_{n=20}(\lambda > 8) \approx 0$ for $k = 4$; and $f_{n=20}(\lambda = 8) \approx 0.9702$ and $f_{n=20}(\lambda > 8) \approx 0$ for $k = 8$.
- (iii) $f_{n=20}(\lambda = k = 8) > f_{n=20}(\lambda = k = 4) > f_{n=20}(\lambda = k = 2)$.

(iv) For fixed k [$=2$ and 8 in the case of Fig. 9(b)], $f_n(\lambda = k)$ increases as n is increased and $f_n(\lambda > k)$ decreases as n is increased. Thus, $f_n(\lambda)$ tends to the Dirac delta function $\delta_k(\lambda)$ as $n \rightarrow \infty$. As k increases, this regime is quickly reached. This situation is clearly reflected in the inset in part (b), where $f_n(\lambda = k)$ is shown as a function of n for $k = 2$ and 8 . It is also instructive to extend the analysis to the intensities of the secondary maxima $f_n(\lambda = 2k)$ in Fig. 9(b). For this purpose, it is useful to define the following quantities: the fraction of islands of sizes k and $2k$ in the n th layer, $f_n(k, 2k) = f_n(k) + f_n(2k)$; and the ratio $r_n(k, 2k) = f_n(k)/f_n(2k)$. In the case of $k = 2$: $f_{n=2}(2, 4) = 0.3211$ and $r_{n=2}(2, 4) = 2.12$; $f_{n=4}(2, 4) = 0.5320$ and $r_{n=4}(2, 4) = 2.34$; $f_{n=8}(2, 4) = 0.7783$ and $r_{n=8}(2, 4) = 3.22$; $f_{n=12}(2, 4) = 0.8863$ and $r_{n=12}(2, 4) = 4.31$; and $f_{n=20}(2, 4) = 0.9496$ and $r_{n=20}(2, 4) = 6.21$. In the case of $k = 8$: $f_{n=2}(8, 16) = 0.2556$ and $r_{n=2}(8, 16) = 6.45$; $f_{n=4}(8, 16) = 0.4917$ and $r_{n=4}(8, 16) = 9.12$; $f_{n=8}(8, 16) = 0.8309$ and $r_{n=8}(8, 16) = 23.44$; $f_{n=12}(8, 16) = 0.9582$ and $r_{n=12}(8, 16) = 38.93$; and $f_{n=20}(8, 16) = 0.9863$ and

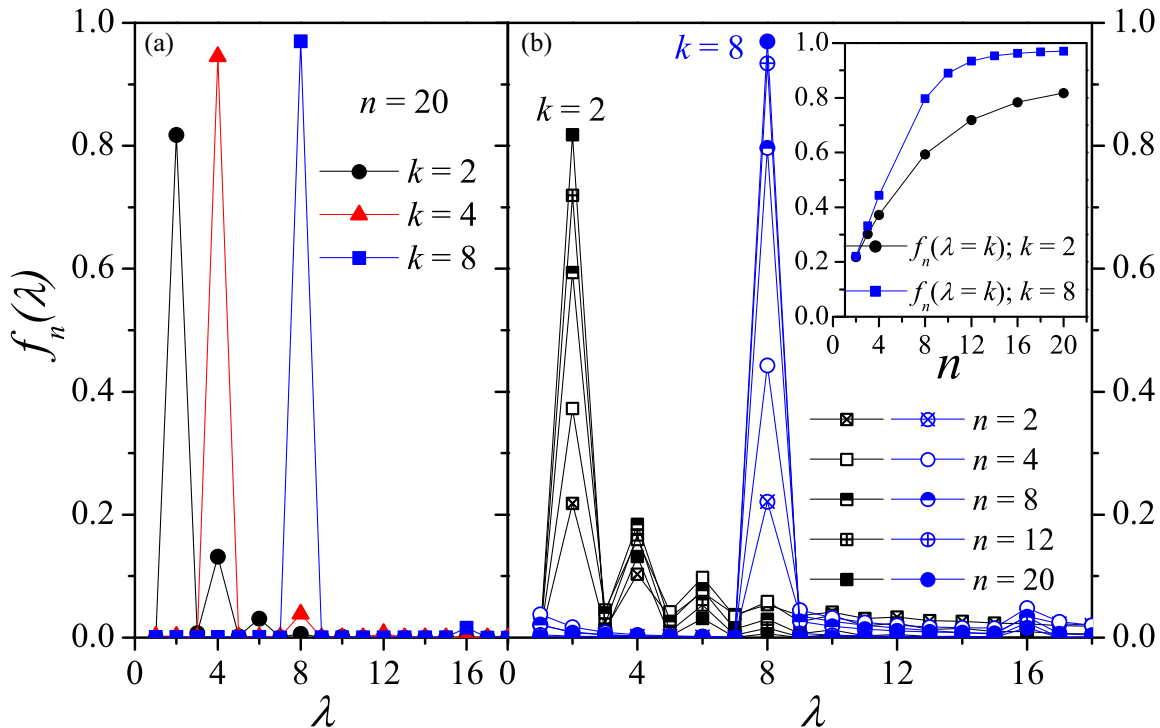


FIG. 9. (a) $f_n(\lambda)$ as functions of the size λ (see the discussion in the text) for three different values of k ($k = 2$, circles; $k = 4$, diamonds; and $k = 8$, triangles) and $n = 20$. (b) Same as (a) for $k = 2$, $k = 8$, and different values of n as indicated. Inset: $f_n(\lambda = k = 2)$ (circles) and $f_n(\lambda = k = 8)$ (squares) vs n .

$r_{n=20}(8, 16) = 60.26$. These indicators show that, for relatively small values of n ($4 \lesssim n \lesssim 8$), the structure of the adsorption state is mainly composed of islands of sizes k and $2k$. As n is increased ($n \gtrsim 8$), islands of size k dominate the adsorption state. The effect is even more marked as the size k is increased.

(v) The case corresponding to $n = 1$ is not included in the figure for the sake of clarity. The first layer state has special characteristics, and it will be discussed in detail in Appendix.

The results (i)–(v) complement the findings obtained from the study in Figs. 7 and 8 and allow us to establish the main features of the filling process at long times (see Fig. 6). In this regime, the incoming k -mers get adsorbed in-registry with previously adsorbed k -mers, forming columns of width k separated by valleys of empty sites. As k increases, the separation distance between columns diminishes [$\theta_\infty^j(k)$ increases with k].

Clearly, the final state of the system ($n \rightarrow \infty$) is governed by the occurrence of the in-registry adsorption phenomenon. Thus, the lower the value of n for which the phenomenon occurs, the higher will be the corresponding value of $\theta_\infty^j(k)$. In fact, as k increases, the value of n for which the limit regime is reached decreases [see the inset of Fig. 9(b)] and $\theta_\infty^j(k)$ increases (see Fig. 8). The ideal/maximum value of $\theta_\infty^j(k)$ would be obtained from the condition of the ideal/minimum value of n ($n = 2$). In this case, k -mers in the upper (second, third, fourth, etc.) layers adsorb exactly onto already adsorbed ones in the first layer, and $\theta_1^j(k) = \theta_n^j(k) = \theta_\infty^j(k)$ [remember that $\theta_1^j(k)$ represents the jamming coverage for the one-dimensional monolayer adsorption problem]. The probability of occurrence of this ideal state tends to zero as L tends to infinity, and consequently (i) the $\theta_\infty^j(k)$ curve remains below $\theta_1^j(k)$ in the entire range of k ; and (ii) the multilayer asymptotic limit $\theta_\infty^j(\infty) \approx 0.71147$ is smaller than the corresponding monolayer asymptotic limit $\theta_1^j(\infty) \approx 0.747598$ (see Fig. 8).

With respect to the jamming critical exponent, a similar study to that shown in Fig. 4 was carried out for different values of k and n (data not shown here for reasons of space). In all cases, the obtained results indicate that ν_j remains close to 2, as expected for a one-dimensional system.

Finally, we briefly refer to the connectivity properties of the system. Even though the limit coverage of the first layer is shifted close to 1 due to the adsorption of k -mer units that have relaxed from the upper layers (see Fig. 7, $n = 1$), jamming transition occurs before the system can reach percolation.

IV. CONCLUSIONS

In this paper, irreversible multilayer adsorption of semi-rigid linear objects of different sizes on one-dimensional lattices has been studied. The adsorption dynamics was modeled by using the random sequential adsorption algorithm.

The process was monitored by following the behavior of the cumulative frequency of the coverage per layer $\Phi_{n,L,k}(\theta_n)$. Cumulative frequency curves for different lattice sizes L cross at precise concentration, allowing us to determine jamming coverage. In addition, by fitting $\Phi_{n,L,k}(\theta_n)$ [$d\Phi_{n,L,k}/d\theta_n$] with the error (Gaussian) function, the maximum of the derivative

of the cumulative frequency $(d\Phi_{n,L,k}/d\theta_n)_{\max}$ and the width of the transition $\Delta_{n,L,k}$ are expected to behave asymptotically as L^{1/ν_j} , which allows for an accurate determination of the jamming exponent ν_j .

We began with numerical simulations for the deposition of dimers on a bilayer, which allowed us to introduce definitions, examples, and they can also be followed by exact enumeration of configurations for small lattices to understand tendencies. Then, we extended the analysis to an increasing number of layers, which is one of the noteworthy aspects of this work: coverage, jamming, percolation, and critical properties were discussed for the multilayer system.

In the bilayer problem, the coverage decreases in both layers as the size k of the deposited particle increases, with a finite value of saturation in the limit of infinitely long k -mers: $\theta_1^j(k) = 0.9644(3) + 0.055(3)/k - 0.027(6)/k^2$ (first layer); $\theta_2^j(k) = 0.5766(4) + 0.545(5)/k - 0.002(10)/k^2$ (second layer); and $\theta_{\text{total}}^j(k) = 0.7708(3) + 0.298(3)/k - 0.011(7)/k^2$ (bilayer). A similar decreasing behavior was found for the standard monolayer problem (or RSA of linear k -mers on one-dimensional lattices) [12–15]. However, some important differences between these systems were observed. Namely, in the bilayer case the deposited particles preferentially fill the first layer leaving empty sites, which are occupied by monomers belonging to k -mers that have relaxed from the second layer. Under these conditions, (i) the limit coverage of the first layer is higher than that corresponding to the monolayer problem in the entire range of k and, (ii) the limit coverage of the second layer is lower than that corresponding to the monolayer problem in the entire range of k . These tendencies were corroborated by measurements on small lattices considering all possible configurations with their exact abundances.

The exact calculations also showed that the percolation probability vanishes as L increases, being zero in the limit $L \rightarrow \infty$. This behavior is expected for one-dimensional systems, where percolation never occurs due to jamming. As introduced by Evans [6], one could think of a “virtual percolation transition” occurring in the unphysical coverage range above jamming. In this case, the jamming coverage of the first layer is shifted close to 1 due to the adsorption of k -mer units that have relaxed from the upper layers, but it is clear that the virtual percolation threshold remains at unity.

To conclude with the analysis of the bilayer problem, the jamming critical exponent ν_j was reported for multilayer adsorption. The obtained value $\nu_j \approx 2$ reveals a simple dependence of this quantity on the dimensionality of the lattice, $\nu_j = 2/d$, and it allows us to generalize recent results found for irreversible monolayer adsorption on Euclidean and fractal lattices [50].

As n increases (multilayer problem), the layer coverage has a strong dependence with the number of layers. For each particle size k , the curve of θ_n^j versus n decreases monotonically toward the upper layers, and it converges to an asymptotic limit as $n \rightarrow \infty$: $\theta_\infty^j(k)$. This limit coverage $\theta_\infty^j(k)$ increases with k . In addition, it reaches a saturation value for very large k -mer sizes ($k \rightarrow \infty$) $\theta_\infty^j(\infty) \approx 0.71147$, which is close to the asymptotic limit for the one-dimensional monolayer adsorption problem $\theta_1^j(k \rightarrow \infty) \rightarrow c_R \approx 0.7475979202$ [12–15].

On the other hand, the number of islands of length λ in each layer was studied. The obtained results indicate that the most abundant island size at any n value is k (the size of the deposited k -mer), followed by multiples of this size, whose abundance decreases rapidly with increasing n . This effect is more marked as the k -mer size increases.

The exhaustive study of the coverage per layer as a function of n , supplemented by the analysis of the number of islands of length in each layer, allowed us to characterize the structure of the adsorbed phase for the problem of irreversible multilayer adsorption of semirigid k -mers deposited on one-dimensional lattices. Thus, as n increases, the $(1 + 1)$ -dimensional adsorbed phase tends to be a “partial wall” consisting of “towers” (or columns) of width k , separated by valleys of empty sites. The separation distance between columns diminishes with increasing k [$\theta_\infty^l(k)$ increases with k]. This resulting structure reveals that the adsorption process is an in-registry adsorption process, where each incoming k -mer gets adsorbed exactly onto an already adsorbed one.

Future efforts will be devoted to extending the present analysis to two-dimensional systems, where the possibility of occurrence of a percolation phase transition opens a challenging field of research.

ACKNOWLEDGMENTS

This work was supported in part by CONICET (Argentina) under Project No. PIP 112-201101-00615, Universidad Nacional de San Luis (Argentina) under Project No. 03-0816, the National Agency of Scientific and Technological Promotion (Argentina) under Project PICT-2013-1678, and Project FONDOCYT-2016-2017-084 Ministry of Higher Education, Science and Technology, MESCYT-Dominican Republic. Ceddenna (Chile) is under contract Conicyt AFB180001 and Fondecyt (Chile) is under contract 1190036. The numerical work was done using the BACO parallel cluster (composed by 50 PCs each with an Intel i7-3370/2600 processor located at Instituto de Física Aplicada, Universidad Nacional de San Luis–CONICET, San Luis, Argentina). N.D.L.C.F. thanks the OAS Academic Scholarship Program (Graduate).

APPENDIX: JAMMING AND PERCOLATION FOR BILAYER ADSORPTION OF SEMIRIGID k -MERS ON ONE-DIMENSIONAL LATTICES: EXACT RESULTS FOR SMALL CELLS

In this Appendix, we will enumerate, in an exhaustive manner, all the possible configurations for deposited semirigid k -mers on small one-dimensional chains in the bilayer regime. To do so, we propose here the following procedure, illustrated in Fig. 10 for deposition of trimers. The figure shows a whole lattice with $L = 9$. The corresponding steps are presented in a general way:

- (i) Consider a lattice of length L being a multiple of k (L/k is an integer).
- (ii) Start with a monolayer exhausting all the possibilities of accommodating k -mers with interspacing varying from zero positions (k -mers touching each other) to $(k - 1)$ positions (larger interspacing spaces would be filled by another k -mer); see Fig. 10(a).

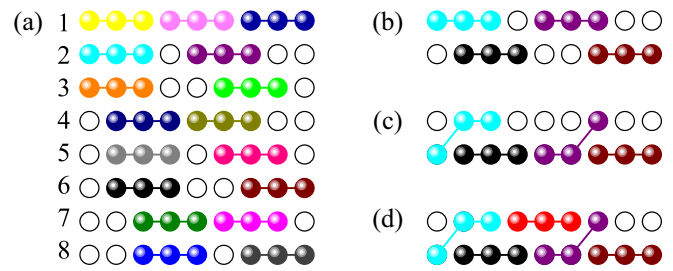


FIG. 10. Process of exhaustive enumeration of all configurations for $L = 9$, $k = 3$, and open boundary conditions. Trimers are represented by solid symbols joined by lines. Empty positions are marked by hollow symbols. (a) All eight possible monolayers; (b) bilayer formed by monolayer no. 2 on top and no. 6 at the bottom; (c) collapse of two atoms leaving three consecutive empty spaces on top; (d) a new trimer is accepted filling the previous three empty positions. This is a final jammed configuration.

- (iii) These configurations are brought together in pairs one on top of the other; see Fig. 10(b).
- (iv) Then, all possible collapses are allowed when an empty position in the lower layer has an occupied position directly above; see Fig. 10(c).
- (v) A refill round follows each collapse round trying to accommodate k -mers in the top layer.
- (vi) This line ends when a jammed configuration is reached after all collapses and refills have been exhausted; see Fig. 10(d).
- (vii) Steps (iv) and (v) are repeated until that particular branch of depositions does not allow further collapses or refills; each final configuration is stored as one possible jammed configuration, a sequential number is assigned, and the configuration of empty and occupied sites is stored.
- (viii) The next branch of depositions is considered (possible in systems larger than the example of Fig. 10) until all of them are exhausted for that particular pair of monolayers.
- (ix) The next pair of monolayers is considered until all pairs of monolayers are processed.

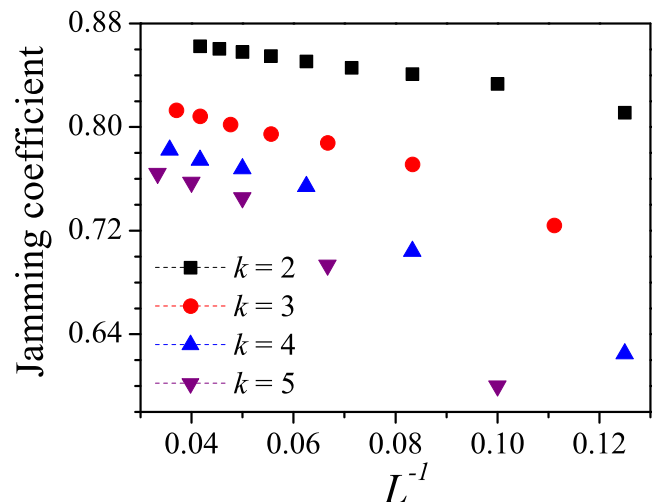


FIG. 11. Jamming concentration as a function of the inverse of L for different k values, as indicated.

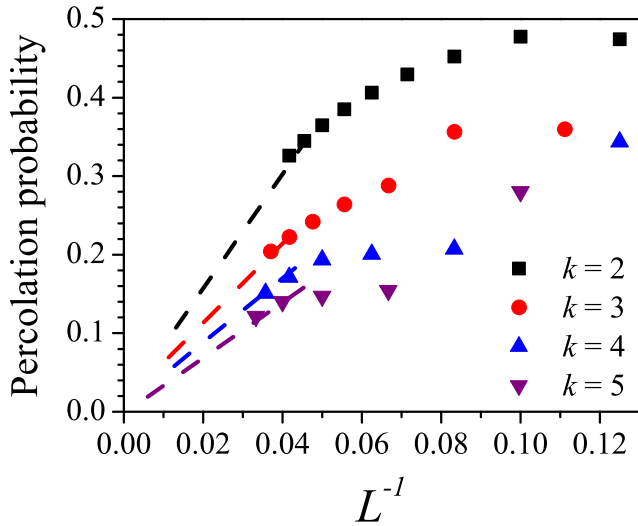


FIG. 12. Percolation probability for layer 1 as a function of the inverse of L for different values of k , as indicated. Dashed lines are extended straight lines joining the points for larger L that are intended only to guide the eye.

This procedure ensures that each possible configuration is present with a probability proportional to the number of independent ways of reaching it. Periodic boundary conditions, used in the numerical simulations presented in Sec. III, are relaxed here, and free (or open) boundary conditions are used without allowing depositions outside the lattice.

The example given in Fig. 10 is one of the 64 possible configurations for $L = 9$ and $k = 3$. This number grows exponentially with L . Thus, for $L = 27$, the total number of configurations for trimer depositions is 1 682 736. Results presented in this Appendix include each one of the possible configurations for each $\{L, k\}$ system reported here.

Since all final concentrations are jammed, we can directly determine the jamming coefficient, equivalent to the jamming coverage $\theta_{\text{total}}^j(L)$ in the simulations, by directly weighting each configuration by the total occupied positions in both layers over $2L$, the total number of available positions. These results are presented in Fig. 11. The resemblance to Fig. 3 is clear with differences coming from finite-size effects. The decrease of the jamming coefficient with k observed in Fig. 11 is also in agreement with the results of the numerical simulations as presented in Fig. 5.

For each given set L, k , it is possible to inquire whether the lower layer percolates or not, since the upper layer could eventually percolate only if the bottom one does. To get this property, each percolating jammed configuration is weighted by its corresponding concentration. This is shown in Fig. 12.

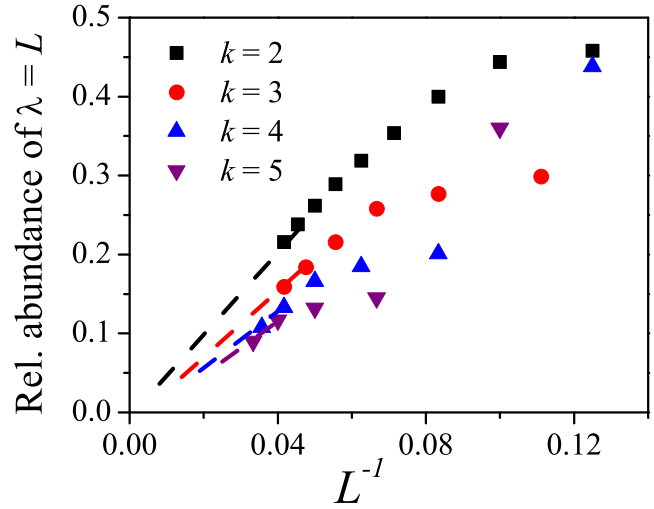


FIG. 13. Relative abundance of the island with length $\lambda = L$ (necessary condition for percolation) as a function of the inverse of L for different k values, as indicated. As in the previous figure, dashed lines are extended straight lines joining the points for larger L that are intended only to guide the eye.

Here we linearly extrapolate the tendencies showing a clear tendency to the origin indicating that percolation points to vanishing in the thermodynamic limit. If a polynomial adjustment is done (not shown in the figures), the intercepts on the ordinate axis for $k = 2, 3, 4$ and 5 are 0.08, 0.00, 0.00, and 0.01, respectively.

To further confirm this result, we studied the length of the islands λ (continuous set of occupied sites) in the lower layer. A necessary condition for percolation is that $\lambda = L$. It is found that $k \leq \lambda < L$ with the exceptions of $\lambda = (2k - 1)$, which is never present due to the deposition rules, and $\lambda = L$, which is only possible for a single ideal configuration with rapidly decreasing probability as L increases (superposition of two filled monolayers). The relative abundance of islands of any length is defined as the number of islands for that λ divided by the total number of islands for all possible λ values. Results for the relative abundance of the percolating island ($\lambda = L$) are shown in Fig. 13. Percolation shows a clear tendency to disappear as L increases.

The results of this Appendix show tendencies that are in agreement with those shown by simulations on larger systems reported in Sec. III A. We do not attempt a fit or matching since simulations were done optimizing results to very large systems, using periodic boundary conditions, aiming for the thermodynamic limit. However, it is encouraging that such results are corroborated by the tendencies shown by analytic results inherent to these systems.

[1] G. Grimmett, *Percolation* (Springer-Verlag, Berlin, 2013).
 [2] A. A. Saberi, *Phys. Rep.* **578**, 1 (2015).
 [3] D. Stauffer and A. Aharony, *Introduction to Percolation Theory* (Taylor & Francis, London, 1994).
 [4] M. Sahimi, *Applications of Percolation Theory* (Taylor & Francis, London, 1994).

[5] J. Feder, *J. Theor. Biol.* **87**, 237 (1980).
 [6] J. W. Evans, *Rev. Mod. Phys.* **65**, 1281 (1993).
 [7] A. Cadilhe, N. A. M. Araújo, and V. Privman, *J. Phys.: Condens. Matter* **19**, 065124 (2007).
 [8] N. A. M. Araújo and A. Cadilhe, *J. Stat. Mech.* (2010) P02019.

- [9] J. J. Gonzales, P. C. Hemmer, and J. S. Hoye, *Chem. Phys.* **3**, 228 (1974).
- [10] A. Karim, V. V. Tsukruk, J. F. Douglas, S. K. Satija, L. J. Fetters, D. H. Reneker, and M. D. Foster, *J. Phys. II France* **5**, 1441 (1995).
- [11] D. Luensmann and L. Jones, *Contact Lens Anterior Eye* **35**, 53 (2012).
- [12] R. H. Swendsen, *Phys. Rev. A* **24**, 504 (1981).
- [13] E. Ben-Naim and P. L. Krapivsky, *J. Phys. A* **27**, 3575 (1994).
- [14] N. O. Wolf, J. W. Evans, and D. K. Hoffman, *J. Math. Phys. (NY)* **25**, 2519 (1984).
- [15] A. Rényi, *Sel. Transl. Math. Stat. Probab.* **4**, 203 (1963) [*Magyar Tud. Akad. Mat. Kutató Int. Közl.* **3**, 109 (1958)].
- [16] J. Becklehimer and R. B. Pandey, *Physica A* **187**, 71 (1992).
- [17] N. Vandewalle, S. Galam, and M. Kramer, *Eur. Phys. J. B* **14**, 407 (2000).
- [18] V. Cornette, A. J. Ramirez-Pastor, and F. Nieto, *Phys. Lett. A* **353**, 452 (2006).
- [19] V. Cornette, A. J. Ramirez-Pastor, and F. Nieto, *J. Chem. Phys.* **125**, 204702 (2006).
- [20] Y. Leroyer and E. Pommiers, *Phys. Rev. B* **50**, 2795 (1994).
- [21] B. Bonnier, M. Hontebeyrie, Y. Leroyer, C. Meyers, and E. Pommiers, *Phys. Rev. E* **49**, 305 (1994).
- [22] G. Kondrat and A. Pękalski, *Phys. Rev. E* **63**, 051108 (2001).
- [23] N. I. Lebovka, N. N. Karmazina, Y. Y. Tarasevich, and V. V. Laptev, *Phys. Rev. E* **84**, 061603 (2011).
- [24] Y. Y. Tarasevich, N. I. Lebovka, and V. V. Laptev, *Phys. Rev. E* **86**, 061116 (2012).
- [25] L. Budinski-Petković, I. Lončarević, M. Petković, Z. M. Jakšić, and S. B. Vrhovac, *Phys. Rev. E* **85**, 061117 (2012).
- [26] L. Budinski-Petković, I. Lončarević, Z. M. Jakšić, and S. B. Vrhovac, *J. Stat. Mech.* (2016) 053101.
- [27] G. D. García, F. O. Sanchez-Varretti, P. M. Centres, and A. J. Ramirez-Pastor, *Eur. J. Phys. B* **86**, 403 (2013).
- [28] E. J. Perino, D. A. Matoz-Fernandez, P. M. Pasinetti, and A. J. Ramirez-Pastor, *J. Stat. Mech.* (2015) P10011.
- [29] M. G. Slutski, L. Yu. Barash, and Yu. Yu. Tarasevich, *Phys. Rev. E* **98**, 062130 (2018).
- [30] S. J. Gregg and K. S. W. Sing, *Adsorption, Surface Area, and Porosity* (Academic, New York, 1991).
- [31] N. Kallay, M. Tomić, B. Biskup, I. Kunjašić, and E. Matijević, *Colloids Surf.* **28**, 185 (1987).
- [32] N. Ryde, N. Kallay, and E. Matijević, *J. Chem. Soc. Faraday Trans.* **87**, 1377 (1991).
- [33] M. F. Haque, N. Kallay, V. Privman, and E. Matijević, *J. Adhes. Sci. Technol.* **4**, 205 (1990).
- [34] V. Privman, N. Kallay, M. F. Haque, and E. Matijević, *J. Adhes. Sci. Technol.* **4**, 221 (1990).
- [35] M. Elimelech and C. R. O'Melia, *Environ. Sci. Technol.* **24**, 1528 (1990).
- [36] J. E. Tobiasson and C. R. O'Melia, *J. Am. Water Works Assoc.* **80**, 54 (1988).
- [37] S. Brunauer, P. H. Emmett, and E. Teller, *J. Am. Chem. Soc.* **60**, 309 (1938).
- [38] J. Frenkel, *Kinetic Theory of Liquids* (Clarendon, Oxford, 1946).
- [39] G. D. Halsey, *J. Chem. Phys.* **16**, 931 (1948).
- [40] T. L. Hill, *Adv. Catal.* **4**, 211 (1952).
- [41] S. Casal, S. H. Wio, and S. E. Mangioni, *Physica A* **311**, 443 (2002).
- [42] F. Romá, A. J. Ramirez-Pastor, and J. L. Riccardo, *Surf. Sci.* **583**, 213 (2005).
- [43] F. O. Sanchez-Varretti, G. D. García, A. J. Ramirez-Pastor, and F. Romá, *J. Chem. Phys.* **130**, 194711 (2009).
- [44] G. D. García, F. O. Sanchez-Varretti, F. Romá, and A. J. Ramirez-Pastor, *Surf. Sci.* **603**, 980 (2009).
- [45] M. C. Bartelt and V. Privman, *J. Chem. Phys.* **93**, 6820 (1990).
- [46] P. Nielaba and V. Privman, *Phys. Rev. A* **45**, 6099 (1992).
- [47] V. Privman and J.-S. Wang, *Phys. Rev. A* **45**, R2155 (1992).
- [48] P. Nielaba, V. Privman, and J.-S. Wang, *Berich. Bunsen. Gesell.* **98**, 451 (1994).
- [49] P. R. Van Tassel and P. Viot, *Europhys. Lett.* **40**, 293 (1997).
- [50] P. M. Pasinetti, L. S. Ramirez, P. M. Centres, A. J. Ramirez-Pastor, and G. A. Cwilich, *Phys. Rev. E* **100**, 052114 (2019).
- [51] L. Kurzawski and K. Malarz, *Rep. Math. Phys.* **70**, 163 (2012).
- [52] J. Hoshen and R. Kopelman, *Phys. Rev. B* **14**, 3438 (1976).